nature photonics

LETTERS

https://doi.org/10.1038/s41566-021-00762-6

Check for updates

A non-unitary metasurface enables continuous control of quantum photon–photon interactions from bosonic to fermionic

Quanwei Li[1,2], Wei Bao[1,2], Zhaoyu Nie[1], Yang Xia[1], Yahui Xue[1], Yuan Wang[1], Sui Yang[1] and Xiang Zhang[1] ✉

Photonic quantum information processing, one of the leading platforms for quantum technologies[1–5], critically relies on optical quantum interference to produce an indispensable effective photon–photon interaction. However, such an effective interaction is fundamentally limited to bunching[6] due to the bosonic nature of photons[7] and the restricted phase response from conventional unitary optical elements[8,9]. Here we propose and experimentally demonstrate a new degree of freedom in the optical quantum interference enabled by a non-unitary metasurface. Due to the unique anisotropic phase response that creates two extreme eigen-operations, we show dynamical and continuous control over the effective interaction of two single photons such that they show bosonic bunching, fermionic antibunching or arbitrarily intermediate behaviour, beyond their intrinsic bosonic nature. This quantum operation opens the door to both fundamental quantum light–matter interaction and innovative photonic quantum devices for quantum communication, quantum simulation and quantum computing.

Metamaterials, structured materials with subwavelength elements, enable wave responses that cannot be found in nature. By tailoring metamaterials, unprecedented properties such as negative refractive indices, sub-diffractional imaging and invisible cloaking have been demonstrated[10–13]. Metasurfaces—two-dimensional metamaterials—allow us to arbitrarily tailor the wave front and propagation of classical light with flat optics[14–18]. At the same time, photons are superb quantum information carriers, due to their long coherence time, room-temperature stability, easy manipulation and light-speed signal transmission. Quantum photonics using single-photon sources, beam-splitters, phase shifters and single-photon detectors has been one of the leading platforms for quantum computation, quantum simulation and quantum communication[1–5]. Consequently, combining metamaterials' unparalleled control of light with quantum optics can lead to unexplored possibilities in quantum information applications[19–22].

The central operation unit in photonic quantum information processing applications such as linear optics quantum computing[1], boson sampling[23,24], quantum walks[25] and quantum communication[26] is quantum two-photon interference (QTPI). The beam-splitter is the key element in this quantum operation. When two indistinguishable single photons arrive simultaneously at the two input ports of a 50:50 beam-splitter, QTPI manifests as the Hong–Ou–Mandel (HOM) effect[6]. In the original HOM experiment, two photons always bunch and leave the beam-splitter in the same output port, generating an effective quantum photon–photon interaction between the two otherwise non-interacting photons. However, the effective photon–photon interaction in QTPI is intrinsically limited to bunching because of the bosonic nature of photons[7] and the fixed phase response of the conventional unitary beam-splitter[8]. As this interaction is the ultimate engine for quantum information processing, the ability to manipulate at will the effective photon–photon interaction in QTPI is crucial and highly desirable[1–5]. Thus far, this challenge has been approached by using necessary additional entanglement resources to construct special input states that are globally symmetric upon exchange to mimic fermionic or anyonic statistics[26–29]. However, such an approach must constrain the quantum statistics across the entire quantum circuit, and local manipulation at the individual beam-splitter level is impossible. Alternative approaches using multiport optical channels or surface plasmons have also been explored, but they are restricted to specific input and output states with extremely limited controllability[30–33]. Therefore, the long-pursued full mastery of the effective quantum photon–photon interaction in QTPI remains a major challenge.

We show a new degree of freedom (DOF) enabled by a non-unitary metasurface that addresses this vital need in quantum optics. We achieve deliberate steering of the critical quantum phase in QTPI that determines the effective interactions of the two single photons, beyond their intrinsic bosonic nature. This is accomplished by subwavelength-scale-designed dual extreme eigen-operations originating from the anisotropic phase response, impossible in conventional optical elements. As an example, here the new synthetic DOF is implemented in the rotational DOF of the metasurface. We experimentally demonstrated that the output of QTPI can be dynamically and continuously directed to be a bunching state, an antibunching state or an arbitrary intermediate state, which can then dictate the effective photon–photon interaction to be boson-like, fermion-like or anyon-like, respectively. Since the two-photon bunching state is maximally entangled and the antibunching state is totally disentangled, the new DOF also manipulates the amount of entanglement between the two photons after postselection. This capability is rooted in the intrinsic phase responses of the non-unitary metasurface itself, which is fundamentally different from the traditional unitary optics. It also eliminates the requirement of extraneous entanglement or specifically selected states. In addition, the control takes effect locally, which is an important increase in flexibility over previous approaches. Importantly, the DOF enables new physics in quantum optical metasurfaces instead of simply repeating or integrating conventional optical components.

[1]Nanoscale Science and Engineering Center (NSEC), University of California, Berkeley, CA, USA. [2]These authors contributed equally: Quanwei Li, Wei Bao.
✉e-mail: xiang@berkeley.edu

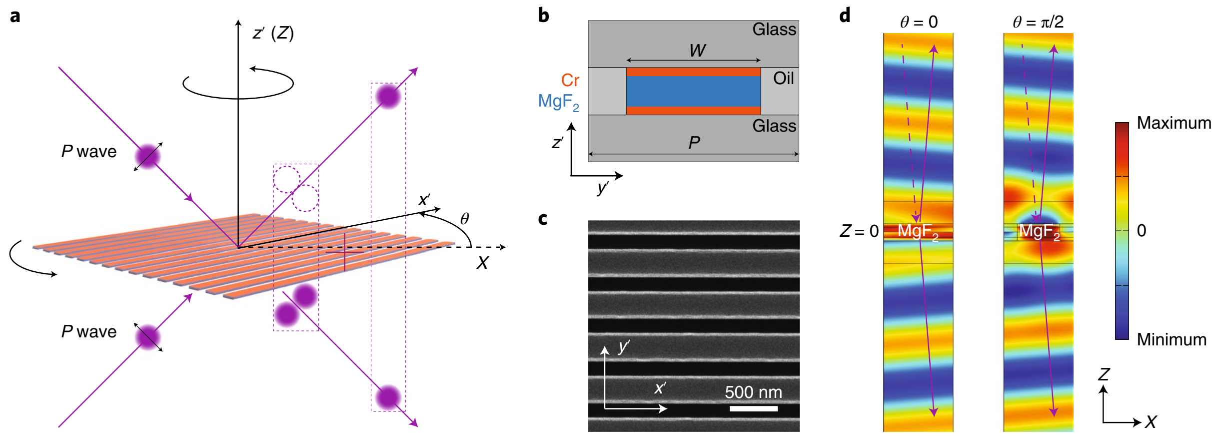

Fig. 1 | Introduction of a new DOF in optical quantum interference by a non-unitary metasurface. a, Given the polarization of the input photons (solid purple balls), for example, P waves, the rotational DOF at the metasurface along its surface normal (z' axis) creates a new synthetic DOF in QTPI. The emergent DOF is specified by the angle θ between the metasurface local x' axis (along the strips) and the laboratory X axis (along the intersection line between the incident plane and the metasurface). The output of QTPI and the associated effective quantum photon–photon interaction can be controlled by changing θ, as illustrated by a superposition of states (dotted rectangles) containing photons (solid purple balls) or no-photons (dotted purple circles). **b**, The metasurface unit structure consists of a three-layer strip made of Cr/MgF_2/Cr (18/59/18 nm) in the z' direction, with 240 nm width (W) and 395 nm period (P) in the y' direction. The strip is sandwiched by two glass plates with index-matching oil filling the gap. **c**, Top-view scanning helium-ion microscope image of the metasurface (typically 36 μm × 36 μm). **d**, The simulated transmitted and reflected magnetic fields' y component (H_y, colour bar) around the metasurface. The reflection plot in $Z > 0$ space is derived by subtracting the incident field from the total field. Arrows indicate the propagation directions.

Incorporating a few such metasurfaces into a large-scale quantum network would dramatically enrich the available quantum operations and quantum functionalities.

The excellent control over the QTPI at the non-unitary metasurface is achieved through designing its anisotropic phase response while simultaneously maintaining a homogeneously constant and balanced amplitude response. To illustrate this (Fig. 1), consider an incident photon with linear polarization P (that is, transverse magnetic mode, defined as the electric field being parallel to the plane of incidence). The metasurface can create a phase difference of zero, $\phi_{rt} \equiv \phi_r - \phi_t = 0$, between the reflection coefficient $r \equiv |r|\mathrm{Exp}(i\phi_r)$ and transmission coefficient $t \equiv |t|\mathrm{Exp}(i\phi_t)$ at a certain designed configuration. When the metasurface rotates 90 degrees along its surface normal, it now produces $\phi_{rt} = \pi/2$ (Fig. 1d). In both cases, the metasurface is designed at the subwavelength scale to maintain $|r| = |t|$. Thus, the metasurface as a symmetric beam-splitter possesses two extreme eigen-operations (Supplementary Notes 4 and 5):

$$\begin{cases} |t|\begin{bmatrix} 1 & 1 \\ 1 & 1 \end{bmatrix}, & \text{at } \theta = 0 \\ |t|\begin{bmatrix} 1 & i \\ i & 1 \end{bmatrix}, & \text{at } \theta = \frac{\pi}{2}, \end{cases} \tag{1}$$

where θ represents the rotation angle of the metasurface along its surface normal (Fig. 1a) and $|t| \le 0.5$ is required in a passive device[34] (Supplementary Note 3 and Supplementary Fig. 8). Note that there are no additional spatial scattering modes in the far fields other than the two inputs and two outputs (Fig. 1d and Supplementary Note 5).

In the HOM-type QTPI experiment[6] with the metasurface, equation (1) can lead to constructive or destructive addition of the probability $P_{(1,1)\mathrm{q}}(\theta)$ for coincidence detection of one single photon at each output port, where the subscript 'q' refers to 'quantum'. Quantitatively, we can write $P_{(1,1)\mathrm{q}}(\theta)$ for the two eigen-operations as the following[7,34] (Supplementary Note 1):

$$P_{(1,1)\mathrm{q}}(\theta) = \left|tt + \mathrm{Exp}\left(i\phi_{\mathrm{qs}}\right)rr\right|^2 = |t|^4\left|1 + \mathrm{Exp}[i\left(\phi_{\mathrm{qs}} + 2\phi_{rt}\right)]\right|^2. \tag{2}$$

As indicated in equation (2), the phase contributions from both quantum statistics, ϕ_{qs} ($\phi_{\mathrm{qs}} = 0$, for photons as bosons; $\phi_{\mathrm{qs}} = \pi$, for fermions), and metasurface response, ϕ_{rt}, govern the final action of QTPI. At arbitrary θ, $P_{(1,1)\mathrm{q}}(\theta)$ can be determined by superposition of the two extreme eigen-operations. Therefore, the rotational DOF θ directly changes ϕ_{rt} and enables us to dictate the effective quantum statistics and effective quantum interactions of the two single photons, beyond their intrinsic bosonic nature.

Furthermore, the correlation among the two photons is important for encoding and processing quantum information[1–5,9]. This correlation can be defined using the second order coherence function $g^{(2)}(\Delta\tau = 0, \theta)$, where $\Delta\tau$ is the delay between two incident photons. We can derive the $g^{(2)}$ in QTPI at the two output ports, which is the normalization of $P_{(1,1)\mathrm{q}}(\theta)$:

$$g^{(2)}(\Delta\tau = 0, \theta) = \frac{P_{(1,1)\mathrm{q}}(\theta)}{P_{(1,1)\mathrm{c}}} = 2\cos^2\theta, \tag{3}$$

where $P_{(1,1)\mathrm{c}}$ represents the classical (as labelled by the subscript 'c') probability of two distinguishable photons, which can be determined at large $\Delta\tau$. Therefore, $g^{(2)}(\Delta\tau = 0) = 1$ means the two photons resemble two classical distinguishable particles, whereas $g^{(2)}(\Delta\tau = 0) < 1$ ($g^{(2)}(\Delta\tau = 0) > 1$) means the two photons tend to bunch (antibunch). It is clear from equations (2) and (3) that the rotational DOF, θ, yields a new synthetic DOF in the QTPI and the effective quantum photon–photon interaction. In stark contrast, only bunching interactions are possible in the original HOM experiment. More details on the theoretical descriptions are presented in Supplementary Note 7. We also note that the presence of loss in the passive metasurface does not affect the QTPI (Supplementary Note 8).

We emphasize that the aforementioned operations are impossible in a conventional symmetric beam-splitter, where the reflection and the transmission coefficients are constrained by the unitary requirement such that the phase difference ϕ_{rt} must be $\pi/2$ (refs. [8,34]) (Supplementary Note 2). To the best of our knowledge, existing conventional optical complement or system cannot satisfy the metasurface operation equations (1) and (3) (Supplementary Note 6).

Table 1 | Response parameters of the metasurface described in the main text

Measurement condition	$\|r\|$	$\|t\|$	$2\phi_{rt}/\pi$
$\theta = 0$	0.305 (0.342)	0.324 (0.338)	0.008 (0.048)
$\theta = \pi/2$	0.336 (0.346)	0.345 (0.364)	0.950 (1.061)

The measured average parameters agree well with the designed values (listed in parentheses). Note that such an anisotropic phase response is highly non-trivial due to the stringent requirements and only possible using a cautiously designed non-unitary metasurface (see text for details). The experimental responses were measured by a homebuilt laser Mach–Zehnder interferometer (Methods, Supplementary Note 10 and Supplementary Figs. 6 and 10), and the designed values were obtained by finite element full-wave simulation (Fig. 1d, Supplementary Note 5 and Supplementary Figs. 2 and 3).

To experimentally demonstrate the new DOF in the QTPI, we designed the metasurface satisfying equation (1). Two configurations with distinct phase responses are needed simultaneously to achieve the two extreme eigen-operations, where the phase control mechanism can originate from either mode resonances of nanostructures or intrinsic properties of materials. The structure consists of an array of subwavelength strips made of ultrathin three-layer Cr/MgF_2/Cr (Fig. 1). The structure was chosen for ease and robustness of fabrication (Supplementary Note 5 and Supplementary Figs. 2 and 12) and subsequently fabricated on top of a transparent substrate using standard nanofabrication techniques (Fig. 1c, Methods and Supplementary Fig. 1). Surprisingly, such a simple structure is highly non-trivial and fulfils the stringently required responses (Fig. 1d). The metasurface responses were experimentally characterized (Supplementary Note 10 and Supplementary Figs. 6 and 10). The measured and designed values of $|r|$, $|t|$ and ϕ_{rt} of the metasurface reported in Table 1 agree well with each other. The linear loss of the passive metasurface can be further reduced to approach the ideal condition $|r| = |t| = 0.5$ by exploring other designs and/or working at a different wavelength (Supplementary Note 5 and Supplementary Fig. 4). In the QTPI experiments, degenerate photon pairs of 710 nm wavelength were produced in spontaneous parametric down-conversion from a BBO crystal (Methods and Supplementary Fig. 5) and then coupled to a two-photon interferometer. The polarization of each photon was set to be P waves before incidence onto the metasurface at a small angle. Finally, the coincidence counts from two outputs were measured as a function of the delay between the two input photons (Methods and Supplementary Fig. 7).

The unique eigen-operations of the metasurface were directly reflected in our QTPI experiments. A completely destructive quantum interference, as in the original HOM effect, was observed at $\theta = \pi/2$, where the two photons always bunch together (Fig. 2a). This was verified by the clear dip of about 0.35 in the measured $g^{(2)}(\Delta\tau)$ at $\Delta\tau = 0$, well below the quantum limit of 0.5 (Fig. 2d). Typically, this is attributed to the bosonic statistics of photons, where the output two-photon state is maximally entangled after postselection. In contrast, at $\theta = 0$, the metasurface yielded completely constructive interference for detecting two photons at separate output ports (Fig. 2c). In this case, the $g^{(2)}(\Delta\tau)$ shows a clear peak of about 1.71 at $\Delta\tau = 0$, well above the quantum limit of 1.5 (Fig. 2f). This indicates that the two photons always antibunch, which resembles fermionic statistics and represents a totally disentangled state after postselection. The theoretical probabilities for all possible outcomes of the two eigen-operations are presented in Supplementary Table 2, distinct from previous approaches using entanglement. At $\theta = \pi/4$, the two eigen-operations were equally superimposed (Fig. 2b) and the

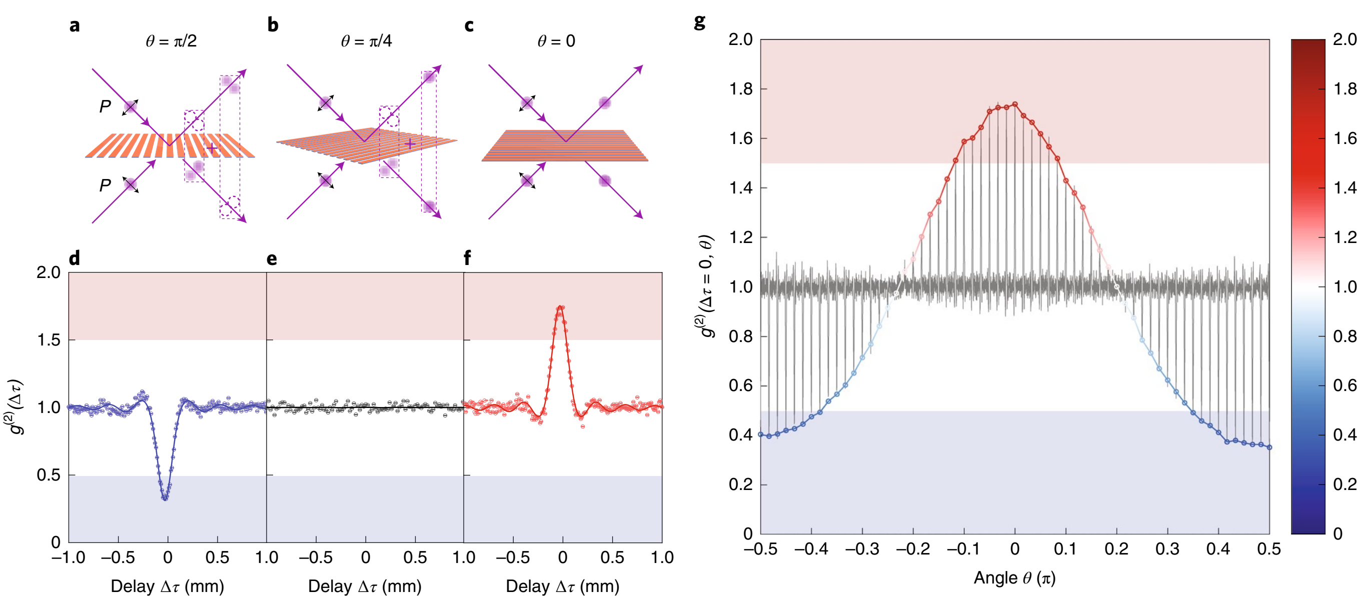

Fig. 2 | Experimental realization of the new DOF in the QTPI. a–c, Schematics of the distinct QTPI output states (as illustrated by the photons (solid purple balls) or no-photons (dotted purple circles) and associated dotted rectangles) at zero delay when the angle θ is equal to $\pi/2$, $\pi/4$ and 0, respectively, corresponding to the postselected bunching state (maximally entangled) and bosonic interaction (**a**), one of the intermediate states (partially entangled) and anyon-like interaction (**b**) and the antibunching state (totally disentangled) and fermion-like interaction (**c**). **d–f**, The measured $g^{(2)}(\Delta\tau)$ between the two identical input photons in HOM-type coincidence measurements for the three cases in (**a–c**). The circles in (**d–f**) are the measured data with error bars (smaller than the circles) calculated assuming the Poisson distribution of event detection, and the solid curves are their fits. **g**, The measured $g^{(2)}(\Delta\tau = 0, \theta)$ as a function of the rotation angle θ enabled by the new DOF, simulating the continuous transition of effective quantum photon–photon interaction from bosonic bunching to fermionic antibunching. The open circle data points (coloured according to the colour bar) are extracted from 61 individual $g^{(2)}(\Delta\tau, \theta)$ curves at each θ value (the catenated grey curves). In **d–g**, the fitted $g^{(2)}(\Delta\tau = 0)$ values have an uncertainty of ± 0.03 at the 95% confidence level and the shaded areas mark the regions arising from the pure quantum effect.

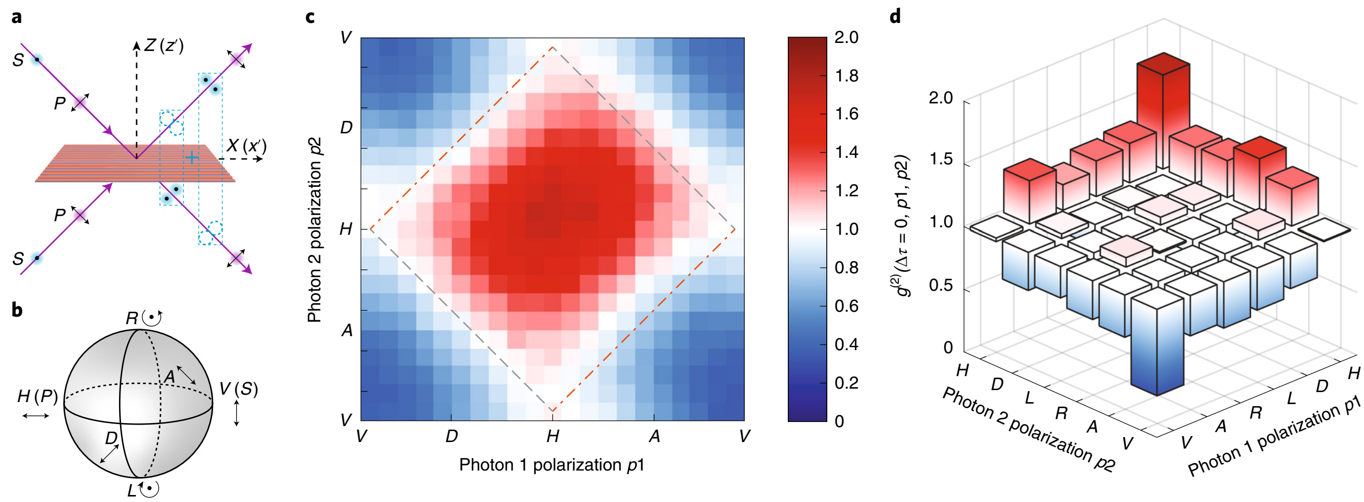

Fig. 3 | The generalized QTPI for independent photon polarizations. **a**, Schematics of the measurement where the metasurface is fixed at $\theta = 0$, while the polarization states of the two incident photons were regulated independently. The case with both photons polarized in P (S) wave is illustrated by purple (blue) balls or circules and associated dotted rectangles. **b**, The Bloch sphere representation of the polarization state where the P (S) wave is defined as the H (V) state. The six representative states H (horizontal), V (vertical), D (diagonal), A (anti-diagonal), L (left circular) and R (right circular) are labelled. **c**, The measured $g^{(2)}(\Delta\tau = 0, p_1, p_2)$ map as a function of the polarizations of the two photons, showing a rich texture and a continuous transition from bosonic bunching to fermionic antibunching. The white regions marked by grey dashed lines correspond to no interference when the two photons have orthogonal polarization, whereas the white regions marked by red dash–dot lines correspond to a balanced superposition of the two extreme eigen-operation interferences. A small shift of the white regions with respect to the dashed lines is due to the imperfection of wave plates. **d**, The measured $g^{(2)}(\Delta\tau = 0, p_1, p_2)$ values with the two photons in the six representative states H, V, D, A, L and R. In **c**–**d**, the fitted $g^{(2)}(\Delta\tau = 0)$ values have an uncertainty of ± 0.03 at the 95% confidence level.

measured flat $g^{(2)}(\Delta\tau)$ (Fig. 2e) simulated one kind of anyonic statistics[29,35], which must be distinguished from the case of no quantum interference between two distinguishable particles. It is also worth noting that the physics is completely classical when antibunching occurs through a 100% reflective beam-splitter or Mach–Zehnder interferometer[36], where no quantum interference effect exists (Supplementary Note 9).

The power of optical quantum computation and quantum simulation relies on harnessing the massively parallel quantum superposition of interacting photons. Well beyond bunching and antibunching states, the new DOF can control the QTPI output in arbitrarily intermediate superposition states. As we adjusted θ continuously from $-\pi/2$ to $\pi/2$, the measured $g^{(2)}(\Delta\tau = 0, \theta)$ evolved continuously from less than 0.5 to greater than 1.5 (Fig. 2g), indicating that the postselected output state changed from bunching (boson-like) to intermediate (anyon-like) to antibunching (fermion-like). Meanwhile, the output state transformed from maximally entangled to totally disentangled. We emphasize that the QTPI at any angle θ other than 0 or $\pi/2$ is a superposition of the two eigen-operations, determined from the rotation angle θ (Supplementary Note 7). These measurements corresponded well with the theoretical predictions from equation (3).

With respect to photonic quantum technologies, polarization is an equally important photon DOF. Conventionally, only the polarization difference is important in QTPI, in contrast with specific polarization values. In previous works, polarization merely assists in forming special wave functions of entangled photon pairs[26–29]. In our case of the unique metasurface, the polarization DOF of each photon can be utilized to encode more information. We performed QTPI measurements with independently controlled photon polarizations (Fig. 3a,b) while keeping $\theta = 0$. This allowed us to map $g^{(2)}(\Delta\tau = 0, p_1, p_2)$ as a function of the two photons polarizations p_1 and p_2 (Fig. 3c), yielding an abundant $g^{(2)}$ texture that depends on the specific photon polarizations, as opposed to only the difference (equation S36). This enriched QTPI and resultant effective quantum photon–photon interaction can bring new quantum functionalities[26,37]. We note two sets of white regions in the map: the regions denoted by two grey dashed lines correspond to situations without interference when the two photons have orthogonal polarizations, whereas the regions denoted by red dash–dot lines correspond to a balanced superposition of the two eigen-cases. More measurements involving circular polarizations are shown in Supplementary Fig. 11. For an overall picture of QTPI with all possible photon polarizations, we further measured the $g^{(2)}(\Delta\tau = 0, p_1, p_2)$ where photon polarizations were independently chosen from the six representative points on their Bloch sphere, that is, H, V, D, A, L and R (Fig. 3d). This represented a variety of QTPI as well as no interference when photon states are orthogonal. The associated effective quantum photon–photon interaction can be derived to be bunching, antibunching or neutral.

To conclude, our non-unitary metasurface enabled a new DOF and novel physics in quantum optics. Strikingly, it allows for dynamical and continuous control over the output quantum state and the effective quantum interaction of the two single photons at will, easily programmed at each such metasurface. Importantly, the new DOF can be utilized to distinguish between polarization-entangled states $|\Phi^+\rangle$ and $|\Phi^-\rangle$ for Bell-state analysis in quantum communication, an impossible task in linear optics without nonlinear elements or additional entanglement[26]. Moreover, the DOF can be used for entanglement filtering[37], a fundamentally non-unitary operation. Furthermore, the non-unitary metasurface presents a platform for studying the dynamics and decoherence of open quantum systems with controlled interaction with environment or loss. In addition, the boson sampling can be upgraded to incorporate fermionic and anyonic behaviours. Such unequalled expansion could enable new possibilities of quantum simulations for molecular vibronic spectra[38] or complex wave functions in quantum chemistry[3]. Similarly, innovative quantum walks would become possible by introducing this new DOF[28]. More photons and/or their other DOFs such as angular momentum[39] or additional spatiotemporal DOFs of metasurfaces[40–42] could be further exploited to empower extraordinary quantum technologies.

Online content

Any methods, additional references, Nature Research reporting summaries, source data, extended data, supplementary information, acknowledgements, peer review information; details of author contributions and competing interests; and statements of data and code availability are available at https://doi.org/10.1038/s41566-021-00762-6.

Received: 10 July 2020; Accepted: 11 January 2021;
Published online: 11 February 2021

References

1. Knill, E., Laflamme, R. & Milburn, G. J. A scheme for efficient quantum computation with linear optics. *Nature* **409**, 46–52 (2001).
2. O'Brien, J. L., Furusawa, A. & Vučković, J. Photonic quantum technologies. *Nat. Photon.* **3**, 687–695 (2009).
3. Aspuru-Guzik, A. & Walther, P. Photonic quantum simulators. *Nat. Phys.* **8**, 285–291 (2012).
4. Walmsley, I. A. Quantum optics: science and technology in a new light. *Science* **348**, 525–530 (2015).
5. Wang, J. et al. Multidimensional quantum entanglement with large-scale integrated optics. *Science* **360**, 285–291 (2018).
6. Hong, C. K., Ou, Z. Y. & Mandel, L. Measurement of subpicosecond time intervals between two photons by interference. *Phys. Rev. Lett.* **59**, 2044–2046 (1987).
7. Loudon, R. Fermion and boson beam-splitter statistics. *Phys. Rev. A* **58**, 4904–4909 (1998).
8. Zeilinger, A. General properties of lossless beam splitters in interferometry. *Am. J. Phys.* **49**, 882–883 (1981).
9. Mandel, L. & Wolf, E. *Optical Coherence and Quantum Optics* (Cambridge Univ. Press, 1995).
10. Pendry, J. B. Negative refraction makes a perfect lens. *Phys. Rev. Lett.* **85**, 3966–3969 (2000).
11. Shelby, R. A., Smith, D. R. & Schultz, S. Experimental verification of a negative index of refraction. *Science* **292**, 77–79 (2001).
12. Fang, N., Lee, H., Sun, C. & Zhang, X. Sub-diffraction-limited optical imaging with a silver superlens. *Science* **308**, 534–537 (2005).
13. Pendry, J. B., Schurig, D. & Smith, D. R. Controlling electromagnetic fields. *Science* **312**, 1780–1782 (2006).
14. Yu, N. et al. Light propagation with phase discontinuities: generalized laws of reflection and refraction. *Science* **334**, 333–337 (2011).
15. Ni, X., Emani, N. K., Kildishev, A. V., Boltasseva, A. & Shalaev, V. M. Broadband light bending with plasmonic nanoantennas. *Science* **335**, 427–427 (2012).
16. Shitrit, N. et al. Spin-optical metamaterial route to spin-controlled photonics. *Science* **340**, 724–726 (2013).
17. Lin, D., Fan, P., Hasman, E. & Brongersma, M. L. Dielectric gradient metasurface optical elements. *Science* **345**, 298–302 (2014).
18. Arbabi, A., Horie, Y., Bagheri, M. & Faraon, A. Dielectric metasurfaces for complete control of phase and polarization with subwavelength spatial resolution and high transmission. *Nat. Nanotechnol.* **10**, 937–943 (2015).
19. Stav, T. et al. Quantum entanglement of the spin and orbital angular momentum of photons using metamaterials. *Science* **361**, 1101–1104 (2018).
20. Wang, K. et al. Quantum metasurface for multiphoton interference and state reconstruction. *Science* **361**, 1104–1108 (2018).
21. Georgi, P. et al. Metasurface interferometry toward quantum sensors. *Light Sci. Appl.* **8**, 70 (2019).
22. Li, L. et al. Metalens-array-based high-dimensional and multiphoton quantum source. *Science* **368**, 1487–1490 (2020).
23. Aaronson, S. & Arkhipov, A. The computational complexity of linear optics. In *Proceedings of the Forty-third Annual ACM Symposium on Theory of Computing* 333–342 (ACM, 2011).
24. Spring, J. B. et al. Boson sampling on a photonic chip. *Science* **339**, 798–801 (2013).
25. Perets, H. B. et al. Realization of quantum walks with negligible decoherence in waveguide lattices. *Phys. Rev. Lett.* **100**, 170506 (2008).
26. Michler, M., Mattle, K., Weinfurter, H. & Zeilinger, A. Interferometric Bell-state analysis. *Phys. Rev. A* **53**, R1209–R1212 (1996).
27. Kwiat, P. G., Steinberg, A. M. & Chiao, R. Y. Observation of a 'quantum eraser': a revival of coherence in a two-photon interference experiment. *Phys. Rev. A* **45**, 7729–7739 (1992).
28. Sansoni, L. et al. Two-particle bosonic-fermionic quantum walk via integrated photonics. *Phys. Rev. Lett.* **108**, 010502 (2012).
29. Matthews, J. C. F. et al. Observing fermionic statistics with photons in arbitrary processes. *Sci. Rep.* **3**, 1539 (2013).
30. Crespi, A. et al. Suppression law of quantum states in a 3D photonic fast fourier transform chip. *Nat. Commun.* **7**, 10469 (2016).
31. Defienne, H., Barbieri, M., Walmsley, I. A., Smith, B. J. & Gigan, S. Two-photon quantum walk in a multimode fiber. *Sci. Adv.* **2**, e1501054 (2016).
32. Wolterink, T. A. W. et al. Programmable two-photon quantum interference in 10^3 channels in opaque scattering media. *Phys. Rev. A* **93**, 053817 (2016).
33. Vest, B. et al. Anti-coalescence of bosons on a lossy beam splitter. *Science* **356**, 1373–1376 (2017).
34. Barnett, S. M., Jeffers, J., Gatti, A. & Loudon, R. Quantum optics of lossy beam splitters. *Phys. Rev. A* **57**, 2134–2145 (1998).
35. Wilczek, F. Quantum mechanics of fractional-spin particles. *Phys. Rev. Lett.* **49**, 957–959 (1982).
36. Silverstone, J. W. et al. On-chip quantum interference between silicon photon-pair sources. *Nat. Photon.* **8**, 104–108 (2014).
37. Okamoto, R. et al. An entanglement filter. *Science* **323**, 483–485 (2009).
38. Huh, J., Guerreschi, G. G., Peropadre, B., McClean, J. R. & Aspuru-Guzik, A. Boson sampling for molecular vibronic spectra. *Nat. Photon.* **9**, 615–620 (2015).
39. Pan, J. W. et al. Multiphoton entanglement and interferometry. *Rev. Mod. Phys.* **84**, 777–838 (2012).
40. Wang, J., Sciarrino, F., Laing, A. & Thompson, M. G. Integrated photonic quantum technologies. *Nat. Photon.* **14**, 273–284 (2020).
41. Hess, O. et al. Active nanoplasmonic metamaterials. *Nat. Mater.* **11**, 573–584 (2012).
42. Shaltout, A. M., Shalaev, V. M. & Brongersma, M. L. Spatiotemporal light control with active metasurfaces. *Science* **364**, eaat3100 (2019).

Methods

Fabrication of the metasurface. The metasurface is fabricated using standard nanofabrication facilities and processes. The fabrication procedure begins with a 1 mm thick, 1 inch diameter NBK7 glass plate with antireflection coating on one side (Thorlabs standard B-coating). On the bare side of the glass plate, an electron beam evaporation system (CHA Solution) is used to consecutively deposit chromium, magnesium fluoride and chromium thin films with thicknesses of 18 nm, 59 nm and 18 nm, respectively. The deposition speeds are 0.04 nm s^{-1} for chromium and 0.46 nm s^{-1} for magnesium fluoride. The thickness of the thin films deposited is strictly calibrated and checked with atomic force microscopy (Park Systems NX20) prior to the real sample deposition.

Metasurface structures are patterned by gallium focused ion beam milling using a Zeiss ORION NanoFab triple beam helium/neon/gallium ion microscope with a current of 100 pA at 30 kV. Pattern files generated using MATLAB are loaded as bitmaps into the NanoPatterning and Visualization Engine (NPVE) from Fibics Inc. The patterned structure is imaged using the helium-ion beam (1 pA, 25 keV). The patterned area is typically 36 μm by 36 μm.

Finally, all the metasurface layers are sealed by another 1 mm thick NBK7 glass plate on top by Kapton tape, with gaps filled by standard index-matching oil TDE (2,2'-thiodiethanol, Sigma-Aldrich). Thus, the final metasurface device is symmetric and can be simply handled as standard 1 inch round optics.

Generation of the two-photon pairs. Degenerate photon pairs at a 710 nm wavelength are produced in spontaneous parametric down-conversion from a BBO crystal (CASTECH) with Type II phase matching, pumped by a 355 nm CW laser (Coherent Genesis CX355-250). The photon pairs pass through long-pass filters blocking the pump residue and an additional 4 nm interference filter (Chroma) on each photon before coupling into single-mode fibres.

Measurements of the QTPI. The two photons from single-mode fibres are directed into a homebuilt two-photon interferometer for the coincidence counts measurements. The polarization of each photon is controlled by a set consisting of a polarizing beam-splitter, half waveplate and quarter waveplate before incident onto the metasurface beam-splitter. The photons are incident at a small angle (7 degrees at the air–glass interface). A tunable delay is introduced into one of the incident photons through a programmable motorized linear stage (Thorlabs). Finally, the output photons from the metasurface are collected using two multimode fibres connected to single-photon counting modules (SPCMs, Excelitas) for coincidence counts measurements (PicoQuant PicoHarp 300).

Characterization of the metasurface. The same two-photon interferometer setup is modified for laser Mach–Zehnder interference measurement to extract the phase response of the metasurface, as well as its reflection and transmission. This is accomplished by replacing the two-photon source with a 710 nm laser (Coherent Chameleon Ultra II) plus a 50:50 beam-splitter and replacing the two SPCMs with two silicon photon detectors (Thorlabs). The signals from the silicon detectors are acquired with data acquisition electronics (National Instruments).

Data availability

The data that support the plots within this paper and other findings of this study are available from the corresponding author upon reasonable request.

Acknowledgements

We thank B. Whaley and H. Haffner for reading of the manuscript and valuable comments. Q.L. also thanks Coherent for loaning the Genesis CX355-250 laser used in the experiments. This work is supported by the Gordon and Betty Moore Foundation and the King Abdullah University of Science and Technology Office of Sponsored Research (OSR) (award OSR-2016-CRG5-2950-03). We acknowledge the facility support at the Biomolecular Nanotechnology Center/QB3 at UC Berkeley. We also acknowledge the facility support at the Molecular Foundry. Work at the Molecular Foundry was supported by the Office of Science, Office of Basic Energy Sciences, of the U.S. Department of Energy under Contract No. DE-AC02-05CH11231.

Author contributions

Q.L., W.B. and X.Z. conceived the idea and initiated the project. Q.L. formulated the theories. Q.L. and W.B. designed the metasurface. Z.N., W.B. and Q.L. fabricated the metasurface with assistance from Y. Xia and Y. Xue. Q.L. designed and built the setup and performed all measurements. Q.L., W.B. and X.Z. analysed the data. Q.L., W.B. and X.Z. wrote the manuscript with assistance from all authors. X.Z., S.Y. and Y.W. supervised the project.

Competing interests

The authors declare no competing interests.

Additional information

Supplementary information The online version contains supplementary material available at https://doi.org/10.1038/s41566-021-00762-6.

Correspondence and requests for materials should be addressed to X.Z.

Peer review information *Nature Photonics* thanks Mark Brongersma, Jianwei Wang and the other, anonymous, reviewer(s) for their contribution to the peer review of this work.